

# Effect of strain rates on deformation behaviors of an in situ Ti-based metallic glass matrix composite

Z. M. Jiao<sup>1</sup> · Z. H. Wang<sup>1</sup> · M. Y. Chu<sup>2</sup> · Y. S. Wang<sup>2</sup> · H. J. Yang<sup>2</sup> · J. W. Qiao<sup>1,2</sup>

Received: 17 March 2016 / Accepted: 11 May 2016 / Published online: 18 May 2016  
© Springer-Verlag Berlin Heidelberg 2016

**Abstract** Quasi-static and dynamic deformation behaviors of an in situ dendrite-reinforced metallic glass matrix composite:  $\text{Ti}_{56}\text{Zr}_{18}\text{V}_{10}\text{Cu}_4\text{Be}_{12}$  were investigated. Upon quasi-static compression, the composite exhibits distinguished work hardening, accompanied by the ultimate strength of 1290 MPa and the plasticity of 20 %. The improved plasticity is attributed to the multiplication of shear bands within the glass matrix and pileups of dislocations within the dendrites. Upon dynamic compression, the stable plastic flow prevails and the yielding stress increases with the strain rate. The macroscopic plasticity decreases considerably, since the shear bands cannot be effectively hindered by dendrites with deteriorated toughness. The dendrite-dominated mechanism results in the positive strain-rate sensitivity, and the Cowper–Symonds model is employed to depict the strain-rate dependency of yielding strength.

## 1 Introduction

Due to their promising properties, including superior high strength and hardness, large elastic limit, and excellent corrosion and wear resistance [1, 2], bulk metallic glasses (BMGs) hold the potential in a wide range of applications for functional and structural materials. However, almost all the BMGs fail with a catastrophic brittleness upon loading at room temperature due to uninhibited shear-band propagation [3]. To alleviate this fatal problem, the crystalline phases are intentionally introduced into the glass matrix to obtain in situ dendrite-reinforced metallic glass matrix composite (MGMC) [4–9], which combine high strength of the glass matrix and large plasticity of dendrites. The ductile secondary phases precipitated during solidification can effectively homogenize the deformation and facilitate the multiplication of shear bands, thus resulting in improved plasticity [10, 11].

The in situ MGMCs usually exhibit macroscopic plasticity upon quasi-static loading at room temperature, since the dendrites within the glass matrix interact with the multiple shear bands [11, 12]. However, for actual structural engineering applications of these in situ composites, many kinds of extreme conditions other than quasi-static loadings should be appreciated. For instance, they can be subjected to high-speed dynamic loadings [13–20]. Qiao et al. [13] have reported that the in situ Ti-based MGMCs exhibited the positive strain-rate sensitivity (SRS), and the yielding stress was increased with increasing strain rates upon dynamic loading. Similar results of a Ti-based MGMC were found by Wang et al. [18]. However, Chu et al. [16] reported that a negative SRS prevails for an in situ Ti-based MGMC with fine dendrites under dynamic compression. According to the investigation by Qiao et al. [12], Zr-based MGMCs exhibited ultrahigh strength and

---

✉ Z. H. Wang  
wangzh077@163.com

✉ J. W. Qiao  
qiaojunwei@gmail.com

<sup>1</sup> Shanxi Key Laboratory of Material Strength and Structural Impact, Institute of Applied Mechanics and Biomedical Engineering, Taiyuan University of Technology, Taiyuan 030024, China

<sup>2</sup> Laboratory of Applied Physics and Mechanics of Advanced Materials, College of Materials Science and Engineering, Taiyuan University of Technology, Taiyuan 030024, China

considerable plasticity upon quasi-static compressive loading, while brittle fracture occurred upon dynamic loading owing to insufficient time to form profuse shear bands. Meanwhile, Jeon et al. [21] found that the maximum fracture strain in Zr-based MGMCs under dynamic compression accounts to 10 %. Qiao et al. [14] claimed that a Ti-based MGMC exhibits remarkable work-hardening capacity upon dynamic loading, which results from coarsen and high-volume-fractioned dendrites and “ductile framework.” Conversely, the apparent softening behavior appears in an in situ Ti-based MGMC during dynamic plastic flows [18]. These inconsistent results indicate that the dynamic deformation behaviors of in situ MGMCs are influenced by many factors like the compositions and microstructures, which stimulates further investigation to uncover the deformation and fracture mechanisms under high strain rates.

In this study, the deformation behavior of an in situ Ti-based MGMC upon quasi-static and dynamic loadings is investigated by exploring the dependence of the yielding strength and plasticity on the strain rates. The positive SRS in the present composites is qualitatively characterized by comparing the competition between dislocation movement associated with the crystalline dendrites and thermal and structural softening related to the glass matrix. Additionally, the constitutive model is obtained to quantitatively depict the strain-rate dependency of the yielding strength under dynamic compression.

## 2 Experimental

Ingots of a nominal composition:  $\text{Ti}_{56}\text{Zr}_{18}\text{V}_{10}\text{Cu}_4\text{Be}_{12}$  (at.%) were prepared by arc melting the mixture of Ti, Zr, V, Cu, and Be with purity higher than 99.9 % (wt%) under a Ti-gettered argon atmosphere. These ingots were remelted at least four times to ensure the chemical homogeneity. The rodlike samples with 3 mm in diameter and about 85 mm in length were fabricated by casting the molten ingots into a copper mold. The phase of the samples was characterized by X-ray diffraction (XRD). The microstructure of the samples was examined with a

scanning electron microscope (SEM). Cylindrical samples with an aspect ratio of 1:1 were prepared for the quasi-static compression at a strain rate of  $1 \times 10^{-3} \text{ s}^{-1}$  at room temperature. The dynamic loading experiments were conducted on samples with an aspect ratio of 1:1 at room temperature using a split Hopkinson pressure bar (SHPB) apparatus with a momentum trap. A SHPB mainly consisted of input and output bars that were made of the high strength steels, as displayed in Fig. 1. The sample was sandwiched between the input and output bars. The test started when the gas released from the gas chamber propelled the striker bar that impinged on the incident bar, thus producing a compressive pulse. The compressive pulse propagated along the incident bar, the specimen, and the transmitted bar. Some of the incident pulse was reflected back into the incident bar from the input bar–specimen interface. The other part of the incident pulse was transmitted through the specimen into the transmitted bar. The strain gauges mounted on the middle of incident bar and transmission bar were used to measure the incident pulse,  $\varepsilon_i(t)$ , the reflected pulse,  $\varepsilon_r(t)$ , and the transmitted pulse,  $\varepsilon_t(t)$ , respectively. According to the one-dimensional stress wave theory [22], the stress and strain as well as strain rate can be obtained at the stress equilibrium conditions as follows:

$$\sigma(t) = E \frac{A_0}{A} \varepsilon_r(t) \quad (1)$$

$$\varepsilon(t) = -\frac{2C_0}{L_0} \int \varepsilon_r(t) dt \quad (2)$$

$$\dot{\varepsilon}(t) = -\frac{2C_0}{L_0} \varepsilon_r(t) \quad (3)$$

where  $E$  is the elastic modulus of the incident and transmission bars,  $A_0$  and  $L_0$  refer to the cross-sectional area and length of the specimen, respectively,  $A$  is the cross-sectional area of the incident and transmission bars, and  $C_0$  is the longitudinal wave velocity in the bars. Moreover, at each loading rate, the compression tests were reduplicated at least three times to ensure the stability and verify the validity of results. After the quasi-static and dynamic compressions, lateral surfaces and fracture surfaces of the

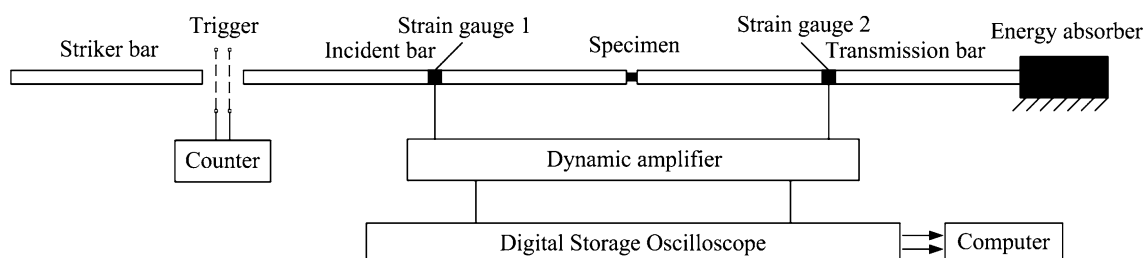


**Fig. 1** Schematic diagram of the split Hopkinson pressure bar (SHPB) and recording system

deformed samples were investigated to identify the deformation and fracture mechanisms by SEM.

### 3 Results

Figure 2 shows the microstructure of the investigated in situ composite. It can be seen that dendrites are homogeneously distributed within the featureless and continuous glass matrix. During cooling of the melt from the high temperature, the embedded dendrites are formed by nucleation and dendritic growth, followed by the solidification of the remaining liquid alloy. The very high volume fraction of the dendritic phase is approximately 65 %, and the average diameter of dendritic arms is about 2  $\mu\text{m}$ . The interconnected dendrites form a continuous network structure. The inset in Fig. 2 presents the XRD pattern, indicating that only the  $\beta$ -Ti crystalline phase with a body-centered-cubic (bcc) structure can be detected. The sharp diffraction peaks of the  $\beta$ -Ti phase are superimposed on the broad diffuse scattering amorphous maxima, which further confirms the dual-phase structure.

Figure 3a displays the engineering stress–strain curve of the composites upon quasi-static compression at a strain rate of  $1 \times 10^{-3} \text{ s}^{-1}$ . It can be found that the yielding strength is 1290 MPa, the ultimate strength is 1930 MPa, and the plasticity prior to failure approaches 20 %. It should be noted that the strength of in situ composites mainly depends on the metallic glass matrix although the volume fraction of dendrites is higher than 70 % [4], since dendrites have much lower strength compared to metallic glass matrix [8]. It is noted that a distinguished work-hardening behavior prevails once the yielding occurs until the final fracture. Analogous phenomena can be found by

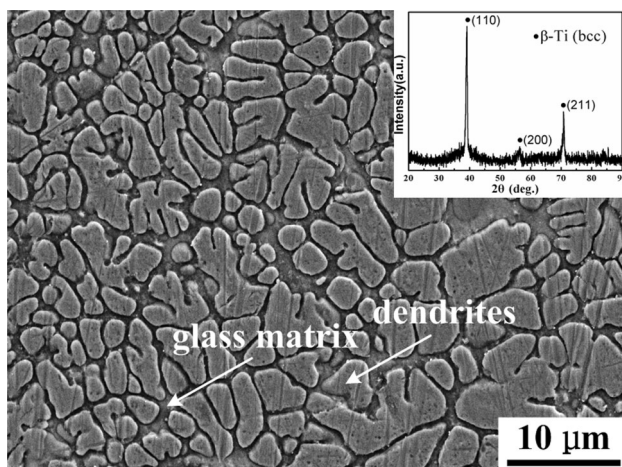


**Fig. 2** Microstructure of the present composite; XRD pattern shown in the *inset*

previous results for in situ MGMCs [12–16]. Generally, multiplication of dislocations within dendrites exists during plastic flows. Severe lattice dislocation and local amorphization in the dendrites, together with pileups of dislocations, occur near the interface between the dendrites and the glass matrix upon straining [14], which are jointly responsible for the accommodation of plastic strains and work hardening under quasi-static compression [23]. To examine the resistance of the present composites to flow localization, the strain-hardening rate (SHR),  $d\sigma/d\varepsilon$  ( $\sigma$  is the flow stress, and  $\varepsilon$  is the plastic strain), as a function of the plastic strain is presented in Fig. 3b. It is found that the SHR values are much higher at the initial plastic stage and decay promptly with the plastic strain, which is markedly less than the reported Zr-/Ti-based MGMCs prepared by four different processes [9].

Figure 3c presents the engineering stress–strain curves upon dynamic compression with varying strain rates in the range of 1400–2800  $\text{s}^{-1}$ . It is apparent that the yielding strengths are over 1350 MPa, a little higher than that under quasi-static compression. All the composites upon varied strain rates exhibit plastic flows [24]. The yielding stress increases slightly but fracture strain decreases with increasing the strain rates, which is consistent with the recent investigations in in situ Ti-based MGMCs [13, 16, 18]. Unlike the quasi-static case, an obvious softening behavior is available after yielding under dynamic compression. However, the improved yielding strength and distinguished plastic flows render this kind of composites promising as engineering materials under dynamic loading. In addition, it is interesting to note that various Young's moduli emerge at different strain rates, since the stress equilibrium cannot be reached instantaneously upon dynamic loading due to the asynchronous response between the load–time and displacement–time [17]. Actually, this phenomenon becomes obvious with increasing the strain rates, which is mainly responsible for decreased modulus under higher strain rates. Under dynamic loading, the corresponding strain rates are essentially constant, as shown in Fig. 3d.

To better understand the deformation mechanisms, it is necessary to analyze the fractographs of the composites. Figure 4a illustrates the lateral surface of the deformed sample upon quasi-static compression. The decrease in length from 3 mm to about 2 mm provides the clear evidence for macroscopic plastic deformation. The fracture plane inclines about  $45^\circ$  with respect to the loading direction, demonstrating that the final fracture occurs along the maximum shear stress direction due to the presence of crystalline dendrites [16]. Profuse shear bands and slip bands, denoted by white and black arrows, respectively, can be observed on the lateral surface, as shown in Fig. 4b,

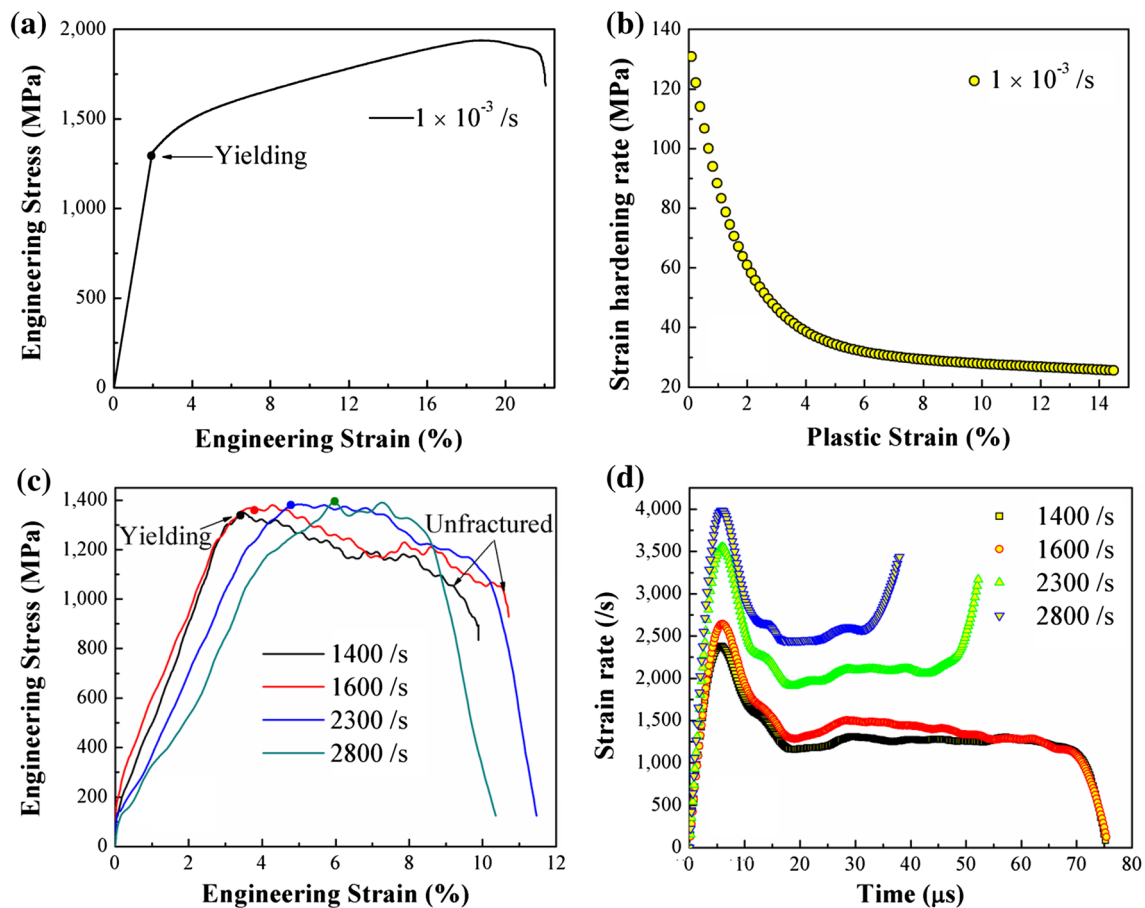


**Fig. 3** Engineering stress–strain curve of the present composite under quasi-static compression (a); the strain-hardening rate as a function of plastic strain upon quasi-static loading (b); the

engineering stress–strain curves under dynamic compression (c); and the strain rates during dynamic loading (d)

which coincides well with the considerable plasticity. The inset in Fig. 4c displays a large plastic deformation of the composites upon dynamic compression. Figure 4c exhibits the lateral surface of the sample under dynamic loading. The prevalence of shear bands and slip bands indicates the effective impediment of dendrites to accommodate the macroscopic deformation [20]. Figure 4d presents the typical fracture surface of the dynamically fractured composites. The abundant resolidified liquid droplets, related to the adiabatic heating [25], and river-like pattern prevail on the fracture surface, mainly associated with the frictional sliding causing a temperature burst sufficiently high to provoke local melting even before fracture [26, 27].

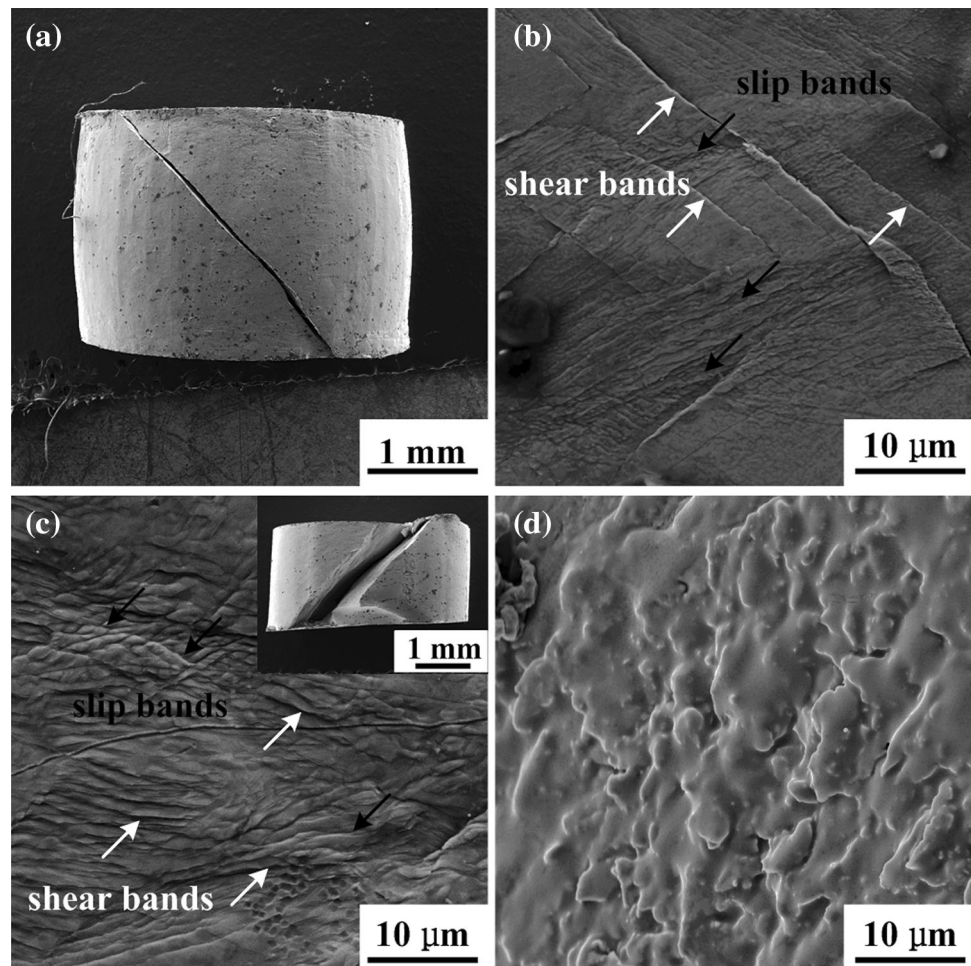
#### 4 Discussion

In general, the deformation mechanisms for the monolithic BMGs and the conventional crystalline alloys are different. For the former, a shear transformation zone (STZ) model is developed to elucidate the plastic deformation of metallic

glasses [28]. According to this model, the shear transformation occurs by spontaneous and cooperative reorganization of a small cluster of randomly close-packed atoms, characterized by the generation of individual shear bands. The large plasticity is usually related to the profuse shear bands [11, 12]. For the latter, the macroscopic plasticity is closely associated with the multiplication of dislocations. As far as the present in situ composites are concerned, the deformation behavior is influenced by the two mechanisms upon quasi-static and dynamic loadings.

Under quasi-static compression, the composite exhibits distinguished work-hardening capacity, accompanied by considerable plasticity. Actually, the work hardening of the ductile dendrites accounts for the macroscopic plasticity, and high strength of the glass matrix is responsible for the large ultimate strength of the composites [15]. Popularly, based on the inconsistent deformation of crystalline dendrites and the glass matrix [8, 29], the deformation behavior of the present composites can be classified into three stages: the elastic stage, plastic stage, and fracture stage. Initially, the applied stress is relatively low, the

**Fig. 4** Lateral surface of the deformed composite under quasi-static compression and the magnified deformation region near the crack shown in **a** and **b**, respectively; the lateral surface and fracture surface under dynamic compression shown in **c** and **d**, respectively. The *inset* in **c** is the macroscopic deformation upon dynamic loading



dendrites and the glass matrix are under elastic deformation, and the dislocations within the dendrites do not glide. At this time, the mismatch in the elastic deformation cannot induce the formation of individual shear bands [11]. Therefore, the composite goes through the elastic stage. When the stress increases to the value where the dislocations within the dendrites start to glide along the easy slide plane, the dendrites begin to yield, and the work hardening appears simultaneously [16]. However, the glass matrix is still under elastic deformation due to its higher strength. As the loading approaches a critical stress value, more and more dislocations gather in the vicinity of the interface, which leads to great stress concentration at the interface and initiation of shear bands within the glass matrix [11]. At this moment, both the dendrites and glass matrix are under plastic deformation. For the composites upon quasi-static compression, the initially nucleated shear bands would propagate along the favorable direction. When the propagation is obstructed by the ductile dendrites, the shear bands either are arrested by the crystalline phases or bypass the barrier wiggly [12]. Consequently, the multiplication of shear bands within the glass matrix as well as pileups of

dislocations within the crystalline dendrites prevails, and the plasticity of the composite is dramatically improved [23]. In addition, the glass matrix exhibits strain softening rather than work hardening after yielding [30]. Once the crystalline dendrites cannot undertake more plastic deformation, further deformation of the composites would be dominated by the glass matrix. Eventually, the shearing failure occurs along the maximum shear stress direction owing to prompt propagation of initially formed shear bands [15, 16].

However, upon dynamic compression, the macroscopic plasticity of the composites decreases considerably due to insufficient time to form multiple shear bands [12]. Chen et al. [19] found that the mismatch between the shear-band toughness of the crystalline dendrites and the glass matrix determines the shear-banding behavior. When subjected to dynamic loading, the higher strain rate leads to the deteriorated toughness of the dendrites. Indeed, the shear bands will be vulnerable to cut through the dendrites rather than be hindered at higher strain rates, responsible for the decreased plasticity compared to quasi-static compression [19]. Upon dynamic loading, the strain accommodation can

be mainly attributed to both coarsen and high-volume-fractioned dendrites and “ductile framework” [14]. For the inhomogeneous deformation in the glass matrix, Spaepen [31] proposed the softening mechanism: if there is to be a lowering of viscosity in the shear bands, there must be an increase in free volumes.

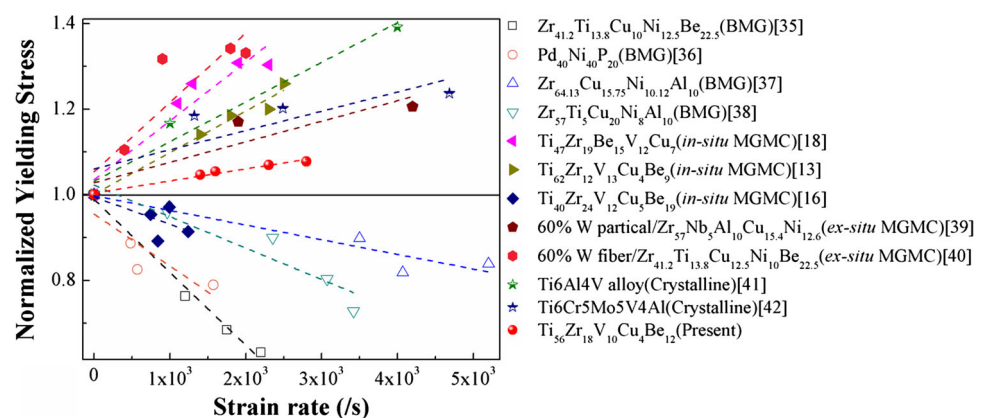
$$\dot{\gamma} = \chi \exp\left(-\frac{\alpha V^*}{V_f}\right) \exp\left(-\frac{\Delta G^m}{RT}\right) \sinh\left(\frac{\tau \lambda \Omega}{2RT}\right) \quad (4)$$

where  $\dot{\gamma}$  is the shear strain rate,  $\chi$  is a factor associated with the amount of the flow units,  $\alpha$  is a constant between 1,  $1/2$ ,  $V^*$  is the effective hard-sphere size of atoms,  $V_f$  is the average free volume of an atom,  $\Delta G^m$  is the thermal activation energy,  $R$  is the gas constant,  $T$  is the absolute temperature, and  $\Omega$  is the molar atom volume. The value of  $\lambda$  is in the range of 0–1. From Eq. (4), it is simply concluded that the higher shear strain rate may induce more creation of free volumes, which facilitates the propagation of shear bands; thus, plasticity is absent for the glass matrix. Therefore, the plasticity is macroscopically accommodated by the “ductile framework,” microscopically characterized by multiple dislocations and severe lattice distortion [13]. For the present composites upon dynamic compression, the rapid propagation of shear bands cannot be effectively arrested by the crystalline dendrites, and individual mature shear bands are available. As a result, the shear cracks would propagate along these mature shear bands and premature failure takes place, which causes the decrease in the plastic strain [15, 16].

Considering the variation of the yielding strength with the strain rates in terms of the present in situ MGMCs, the SRS depends on the competition between the positive effect associated with the dislocation mechanism in the crystalline dendrites and the negative effect related to the thermal and structural softening mechanism in the glass matrix [16, 20]. For the crystalline dendrites, based on the Taylor dislocation theory [32], the relationship between the

critical shear stress of dislocations,  $\tau$  and the average velocity,  $v$  follows  $v = A\tau^m$ , where  $A$  and  $m$  are materials constants. It is noted that the higher strain rate requires higher stress to activate dislocations movement, resulting in a positive SRS. In contrast, for the glass matrix, the critical adiabatic shear deformation exerts a dominant role on the strain-rate-dependent deformation behavior. Larger temperature rising dominates in the critical shear bands at higher strain rates during deformation [33]. Actually, more thermal softening from larger temperature rising further leads to the lower critical shear stress [34], indicating a negative SRS. Figure 5 summarizes the variation of the yielding strength with the strain rate in monolithic BMGs [35–38], in situ and ex situ MGMCs [13, 16, 18, 39, 40], and crystalline alloys [41, 42]. For comparison, the yielding stress has been normalized to the yielding stress for each alloy under quasi-static compression. It can be clearly seen that the BMGs exhibit negative SRS over a wide range of strain rates. Indeed, the yielding strength decreases with increasing strain rates upon dynamic loading, which has been attributed to the dominant thermal softening during dynamic compression [35]. However, for most in situ and ex situ MGMCs by introducing crystalline phases, a positive SRS prevails owing to the dislocation multiplication within the reinforced phases under high strain rates [32, 40]. Furthermore, the in situ  $\text{Ti}_{40}\text{Zr}_{24}\text{V}_{12}\text{Cu}_5\text{Be}_{19}$  composite shows the negative SRS, since the dendrite size of only  $0.3 \mu\text{m}$  is so small that the positive effect of the crystalline dendrites cannot compensate the negative effect of the glass matrix [16]. For comparison, the strain-rate dependence of the crystalline alloys is displayed in Fig. 5. Unlike those monolithic BMGs, these crystalline materials present a positive SRS under dynamic compression. It is noteworthy that the yielding strength increases with increasing strain rates for the current composites, mainly due to the coarse dendritic arms and the high volume fraction of dendrites [13]. Therefore, a

**Fig. 5** Variation of yielding stress (normalized by the yielding stress under quasi-static compression) as a function of strain rate in monolithic BMGs, in situ and ex situ MGMCs, as well as crystalline alloys



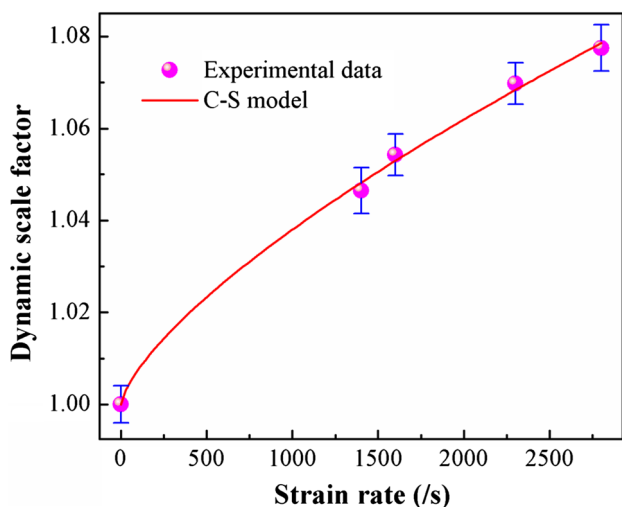


**Fig. 6** Dynamic scale factor for the present composite in compression

positive SRS of the present in situ MGMCs owns the characteristic of the crystalline materials, demonstrating that the crystalline dendrites instead of the glass matrix assume more dominance on the yielding strength at higher strain rates during deformation [20].

For a better understanding of the mechanical properties of the composites, the dynamic scale factor,  $k$ , is used to describe the strain-rate dependency [43]. The yielding strength at the strain rate of  $1 \times 10^{-3} \text{ s}^{-1}$  is used as a reference value, and the yielding strength of the composites under corresponding strain rate is written as  $\sigma_d = k\sigma_s$ , in which  $\sigma_d$  stands for the yielding stress under corresponding strain rate,  $\sigma_s$  represents the referential value of the yielding stress, and  $k$  is the strain-rate function. According to the Cowper–Symonds (C–S) model [44], the  $k$  can be obtained as:

$$k = 1 + \left( \frac{\dot{\varepsilon}}{D} \right)^{1/q} \quad (5)$$

where  $D$  and  $q$  are the two parameters of the model and  $\dot{\varepsilon}$  is the strain rate. After the fitting of the experimental data,  $k$  can be expressed as  $k = 1 + \left( \frac{\dot{\varepsilon}}{103694} \right)^{1/1.42}$ .

In order to testify the validity of the constitutive relationship, experimental yielding stresses and their corresponding C–S model are compared in Fig. 6. A close comparison of the fitting curve and experimental data suggests that the  $k$  faithfully depicts the variation of the yielding stress in relation to that of the strain rate. Therefore, the dynamic scale factor  $k$  reasonably predicts the yielding strength upon dynamic compression for the current composites.

## 5 Conclusion

In conclusion, the compressive deformation behaviors of an in situ Ti-based metallic glass matrix composite/Ti<sub>56</sub>-Zr<sub>18</sub>V<sub>10</sub>Cu<sub>4</sub>Be<sub>12</sub> upon quasi-static and dynamic loadings are investigated. Upon quasi-static compression, the composites exhibit distinguished work-hardening capacity. The ultimate strength is 1290 MPa, and the plasticity approaches 20 % prior to failure. Both the multiplication of shear bands within the glass matrix and pileups of dislocations within the crystalline dendrites are responsible for the improved plasticity. Upon dynamic compression, the stable plastic flows prevail during deformation, and the yielding strength increases with increasing strain rates. Compared to the quasi-static loading, the shear bands cannot be effectively arrested by the crystalline phases and the macroscopic plasticity decreases considerably due to the deteriorated toughness of the dendrites, while the positive strain-rate sensitivity of the yielding strength appears, since the crystalline dendrites assume more dominance on strain-rate effects. The Cowper–Symonds model is employed to describe the strain-rate dependency of the yielding stress, and the dynamic scale factor is obtained for the present composite.

**Acknowledgments** J.W. Q would like to acknowledge the financial support of National Natural Science Foundation of China (No. 51371122), the Program for the Innovative Talents of Higher Learning Institutions of Shanxi (2013), and the Youth Natural Science Foundation of Shanxi Province, China (No. 2015021005). H.J. Y would like to acknowledge the financial support from the National Natural Science Foundation of China (No. 51401141) and the Youth Science Foundation of Shanxi Province, China (No. 2014021017-3). Z.H. W would like to acknowledge the National Natural Science Foundation of China (No. 11390362).

## References

1. M.K. Miller, P.K. Liaw, *Bulk Metallic Glasses* (Springer, New York, 2007)
2. M.M. Trexler, N.N. Thadhani, Mechanical properties of bulk metallic glasses. *Prog. Mater. Sci.* **55**, 759 (2010)
3. A.L. Greer, Y.Q. Cheng, E. Ma, Shear bands in metallic glasses. *Mater. Sci. Eng., R* **74**, 71 (2013)
4. D.C. Hofmann, J.Y. Suh, A. Wiest, G. Duan, M.L. Lind, M.D. Demetriou, W.L. Johnson, Designing metallic glass matrix composites with high toughness and tensile ductility. *Nature* **451**, 1085 (2008)
5. J.W. Qiao, A.C. Sun, E.W. Huang, Y. Zhang, P.K. Liaw, C.P. Chuang, Tensile deformation micromechanisms for bulk metallic glass matrix composites: from work-hardening to softening. *Acta Mater.* **59**, 4126 (2011)
6. R.D. Conner, R.B. Dandliker, W.L. Johnson, Mechanical properties of tungsten and steel fiber reinforced Zr<sub>41.25</sub>Ti<sub>13.75</sub>Cu<sub>12.5</sub>-Ni<sub>10</sub>Be<sub>22.5</sub> metallic glass matrix composites. *Acta Mater.* **46**, 6089 (1998)

7. J.W. Qiao, S. Wang, Y. Zhang, P.K. Liaw, G.L. Chen, Large plasticity and tensile necking of Zr-based bulk-metallic-glass-matrix composites synthesized by the Bridgman solidification. *Appl. Phys. Lett.* **94**, 151905 (2009)
8. C.C. Hays, C.P. Kim, W.L. Johnson, Microstructure controlled shear band pattern formation and enhanced plasticity of bulk metallic glasses containing in situ formed ductile phase dendrite dispersions. *Phys. Rev. Lett.* **84**, 2901 (2000)
9. R.L. Narayan, P.S. Singh, D.C. Hofmann, N. Hutchinson, K.M. Flores, U. Ramamurty, On the microstructure—tensile property correlations in bulk metallic glass matrix composites with crystalline dendrites. *Acta Mater.* **60**, 5089 (2012)
10. J.W. Qiao, T. Zhang, F.Q. Yang, P.K. Liaw, S. Pauly, B.S. Xu, A tensile deformation model for in situ dendrite/metallic glass matrix composites. *Sci. Rep.* **3**, 2816 (2013)
11. T. Zhang, H.Y. Ye, J.Y. Shi, H.J. Yang, J.W. Qiao, Dendrite size dependence of tensile plasticity of in situ Ti-based metallic glass matrix composites. *J. Alloys. Compd.* **583**, 593 (2014)
12. J.W. Qiao, P. Feng, Y. Zhang, Q.M. Zhang, P.K. Liaw, G.L. Chen, Quasi-static and dynamic deformation behaviors of in situ Zr-based bulk-metallic-glass-matrix composites. *J. Mater. Res.* **25**, 2264 (2010)
13. J.W. Qiao, M.Y. Chu, L. Cheng, H.Y. Ye, H.J. Yang, S.G. Ma, Z.H. Wang, Plastic flows of in situ metallic glass matrix composites upon dynamic loading. *Mater. Lett.* **119**, 92 (2014)
14. J.W. Qiao, H.Y. Ye, Y.S. Wang, S. Pauly, H.J. Yang, Z.H. Wang, Distinguished work-hardening capacity of a Ti-based metallic glass matrix composite upon dynamic loading. *Mater. Sci. Eng., A* **585**, 277 (2013)
15. M.Y. Chu, Z.M. Jiao, R.F. Wu, Z.H. Wang, H.J. Yang, Y.S. Wang, J.W. Qiao, Quasi-static and dynamic deformation behaviors of an in situ Ti-based metallic glass matrix composite. *J. Alloys Compd.* **640**, 305 (2015)
16. M.Y. Chu, Z.M. Jiao, Z.H. Wang, Y.S. Wang, J.H. Zhang, H.J. Yang, J.W. Qiao, Different deformation behaviors of two in situ Ti-based metallic glass matrix composites upon quasi-static and dynamic compressions. *Mater. Sci. Eng., A* **639**, 717 (2015)
17. Y.S. Wang, G.J. Hao, J.W. Qiao, Y. Zhang, J.P. Lin, High strain rate compressive behavior of Ti-based metallic glass matrix composites. *Intermetallics* **52**, 138 (2014)
18. Y.S. Wang, G.J. Hao, R. Ma, Y. Zhang, J.P. Lin, Z.H. Wang, J.W. Qiao, Quasi-static and dynamic compression behaviors of metallic glass matrix composites. *Intermetallics* **60**, 66 (2015)
19. J.H. Chen, M.Q. Jiang, Y. Chen, L.H. Dai, Strain rate dependent shear banding behavior of a Zr-based bulk metallic glass composite. *Mater. Sci. Eng., A* **576**, 134 (2013)
20. J. Bai, J.S. Li, J. Wang, J. Cui, L.Y. Li, H.C. Kou, P.K. Liaw, Strain-rate-dependent deformation behavior in a Ti-based bulk metallic glass composite upon dynamic deformation. *J. Alloys Compd.* **639**, 131 (2015)
21. C. Jeon, M. Kang, C.P. Kim, H.S. Kim, S. Lee, Quasi-static and dynamic compressive deformation behaviors in Zr-based amorphous alloys containing ductile dendrites. *Mater. Sci. Eng., A* **579**, 77 (2013)
22. R.W. Armstrong, S.M. Walley, High strain rate properties of metals and alloys. *Int. Mater. Rev.* **53**, 105 (2008)
23. J.W. Qiao, Y. Zhang, P.K. Liaw, G.L. Chen, Micromechanisms of plastic deformation of a dendrite/Zr-based bulk-metallic-glass composite. *Scr. Mater.* **61**, 1087 (2009)
24. Y. Zhang, W.H. Wang, P.K. Liaw, G. Wang, J.W. Qiao, Serration and noise behavior in advanced materials. *J. Iron. Steel Res. Int.* **23**, 1 (2016)
25. C.T. Liu, L. Healthly, D.S. Easton, C.A. Carmichael, J.H. Schneibel, C.H. Chen, J.L. Wright, M.H. Yoo, J.A. Horton, A. Inoue, Test environment and mechanical properties of Zr-base bulk amorphous alloys. *Metall. Mater. Trans. A* **29**, 1811 (1998)
26. S. Cheng, X.L. Wang, H. Choo, P.K. Liaw, Global melting of  $Zr_{57}Ti_5Ni_8Cu_{20}Al_{10}$  bulk metallic glass under microcompression. *Appl. Phys. Lett.* **91**, 201917 (2007)
27. K. Georgarakis, M. Aljerf, Y. Li, A. LeMoulec, F. Charlot, A.R. Yavari, K. Chornokhvosenko, E. Tabachnikova, G.A. Evangelakis, D.B. Miracle, A.R. Greer, T. Zhang, Shear band melting and serrated flow in metallic glasses. *Appl. Phys. Lett.* **93**, 031907 (2008)
28. A.S. Argon, Plastic deformation in metallic glasses. *Acta Metall.* **27**, 47 (1979)
29. C. Fan, R.T. Ott, T.C. Hufnagel, Metallic glass matrix composite with precipitated ductile reinforcement. *Appl. Phys. Lett.* **81**, 1020 (2002)
30. H. Bei, S. Xie, E.P. George, Softening caused by profuse shear banding in a bulk metallic glass. *Phys. Rev. Lett.* **96**, 105503 (2006)
31. F. Spaepen, A microscopic mechanism for steady state inhomogeneous flow in metallic glasses. *Acta Metall.* **25**, 407 (1977)
32. W.G. Johnston, J.J. Gilman, Dislocation velocities, dislocation densities, and plastic flow in lithium fluoride crystals. *J. Appl. Phys.* **30**, 129 (1959)
33. W.D. Liu, K.X. Liu, Dynamic behavior of a Zr-based metallic glass at cryogenic temperature. *Intermetallics* **19**, 109 (2011)
34. W. Zheng, Y.J. Huang, J. Shen, Influence of strain-rate on compressive-deformation behavior of a Zr–Cu–Ni–Al bulk metallic glass at cryogenic temperature. *Mater. Sci. Eng., A* **528**, 6855 (2011)
35. F. Zeng, Y. Chen, M.Q. Jiang, C. Lu, L.H. Dai, Dynamic fragmentation induced by network-like shear bands in a Zr-based bulk metallic glass. *Intermetallics* **56**, 96 (2015)
36. T. Mukai, T.G. Nieh, Y. Kawamura, A. Inoue, K. Higashi, Effect of strain rate on compressive behavior of a  $Pd_{40}Ni_{40}P_{20}$  bulk metallic glass. *Intermetallics* **10**, 1071 (2002)
37. W.D. Liu, K.X. Liu, X.X. Xia, W.H. Wang, The failure stress of bulk metallic glasses under very high strain rate. *J. Mater. Res.* **25**, 1230 (2010)
38. T.C. Hufnagel, T. Jiao, Y. Li, L.-Q. Xing, K.T. Ramesh, Deformation and failure of  $Zr_{57}Ti_5Cu_{20}Ni_8Al_{10}$  bulk metallic glass under quasi-static and dynamic compression. *J. Mater. Res.* **17**, 1441 (2002)
39. T. Jiao, L.J. Kecskes, T.C. Hufnagel, K.T. Ramesh, Deformation and failure of  $Zr_{57}Nb_5Al_{10}Cu_{15.4}Ni_{12.6}/W$  particle composites under quasi-static and dynamic compression. *Metall. Mater. Trans. A* **35**, 3439 (2004)
40. D. Gao, C.H. Guo, F.C. Jiang, G. Chen, The dynamic compressive behavior of  $W_7/Zr$ -based metallic glass composites. *Mater. Sci. Eng., A* **641**, 107 (2015)
41. N. Biswas, J.L. Ding, Numerical study of the deformation and fracture behavior of porous  $Ti_6Al_4V$  alloy under static and dynamic loading. *Int. J. Impact Eng.* **82**, 89 (2015)
42. H. Zhan, D. Kent, G. Wang, M.S. Dargusch, The dynamic response of a  $\beta$  titanium alloy to high strain rates and elevated temperatures. *Mater. Sci. Eng., A* **607**, 417 (2014)
43. A. Brara, J.R. Klepaczko, Experimental characterization of concrete in dynamic tension. *Mech. Mater.* **38**, 253 (2006)
44. G.R. Cowper, P.S. Symonds, Strain hardening and strain rate effect in the impact loading of cantilever beams. Brown University applied mathematics report; report no. 28 (1957)